Lecture Notes in Electrical Engineering 721

Rajeev Agrawal
Chandramani Kishore Singh
Ayush Goyal *Editors*

Advances in Smart Communication and Imaging Systems

Select Proceedings of MedCom 2020

Springer

Lecture Notes in Electrical Engineering

Volume 721

The book series *Lecture Notes in Electrical Engineering* (LNEE) publishes the latest developments in Electrical Engineering - quickly, informally and in high quality. While original research reported in proceedings and monographs has traditionally formed the core of LNEE, we also encourage authors to submit books devoted to supporting student education and professional training in the various fields and applications areas of electrical engineering. The series cover classical and emerging topics concerning:

- Communication Engineering, Information Theory and Networks
- Electronics Engineering and Microelectronics
- Signal, Image and Speech Processing
- Wireless and Mobile Communication
- Circuits and Systems
- Energy Systems, Power Electronics and Electrical Machines
- Electro-optical Engineering
- Instrumentation Engineering
- Avionics Engineering
- Control Systems
- Internet-of-Things and Cybersecurity
- Biomedical Devices, MEMS and NEMS

For general information about this book series, comments or suggestions, please contact leontina.dicecco@springer.com.

To submit a proposal or request further information, please contact the Publishing Editor in your country:

China

Jasmine Dou, Editor (jasmine.dou@springer.com)

India, Japan, Rest of Asia

Swati Meherishi, Editorial Director (Swati.Meherishi@springer.com)

Southeast Asia, Australia, New Zealand

Ramesh Nath Premnath, Editor (ramesh.premnath@springernature.com)

USA, Canada:

Michael Luby, Senior Editor (michael.luby@springer.com)

All other Countries:

Leontina Di Cecco, Senior Editor (leontina.dicecco@springer.com)

**** This series is indexed by EI Compendex and Scopus databases. ****

More information about this series at http://www.springer.com/series/7818

Rajeev Agrawal · Chandramani Kishore Singh · Ayush Goyal
Editors

Advances in Smart Communication and Imaging Systems

Select Proceedings of MedCom 2020

Springer

Editors
Rajeev Agrawal
G. L. Bajaj Institute of Technology and Management
Greater Noida, India

Ayush Goyal
Department of Electrical Engineering and Computer Science
Texas A&M University – Kingsville
Kingsville, TX, USA

Chandramani Kishore Singh
Indian Institute of Science Bangalore
Bengaluru, India

ISSN 1876-1100 ISSN 1876-1119 (electronic)
Lecture Notes in Electrical Engineering
ISBN 978-981-15-9937-8 ISBN 978-981-15-9938-5 (eBook)
https://doi.org/10.1007/978-981-15-9938-5

This Springer imprint is published by the registered company Springer Nature Singapore Pte Ltd.
The registered company address is: 152 Beach Road, #21-01/04 Gateway East, Singapore 189721, Singapore

Preface

Recent advances in different domains like sensor technologies, wireless communications, computer vision medical image, data processing and globalization of digital society across various social areas have intensified the growth of remote healthcare services. However, several socioeconomic aspects and integration of these services with classical healthcare system remain as a challenging issue. In today's context, smart systems are emerging from the integration of embedded computing devices, smart objects, imaging techniques, people and physical environments, which are normally tied by a communication infrastructure. These include systems like smart cities, smart grids, smart factories, smart buildings, smart houses and smart cars where every object is connected to every other object. They are aimed to provide an adaptive, resilient, efficient and cost-effective scenario.

This book presents the selected proceedings of the International Conference on Smart Communication and Imaging Systems (MedCom 2020). It explores the recent technological advances in the field of next-generation communication systems and latest techniques for image processing, analysis and its related applications. The topics include design and development of smart, secure and reliable future communication networks; satellite, radar and microwave techniques for intelligent communication. The book also covers methods and applications of GIS and remote sensing; medical image analysis and its applications in smart health; and other real-life applications of imaging and smart communication. This book can be a valuable resource for academicians, researchers and professionals working in the field of smart communication systems and image processing including artificial intelligence, machine learning and their applications in building smart systems. It will contribute to foster integration of latest and future communication technologies with imaging systems and services, suggesting solutions to various social and techno-commercial issues of global significance.

Greater Noida, India — Rajeev Agrawal
Bengaluru, India — Chandramani Kishore Singh
Kingsville, USA — Ayush Goyal

Contents

About the Editors

Dr. Rajeev Agrawal is currently working as professor and director at G. L. Bajaj Institute of Technology and Management, Greater Noida, India. He has an illustrated experience of more than 25years in teaching and research, holds a B.E. degree in Electronics Engineering and M. Tech. degree in System Engineering. He received Ph.D. in the area of Wireless Communication Channels from School of computer & System sciences, JNU, New Delhi. He was visiting professor at Kennesaw State University, Georgia, USA under a joint research projects in the area of Remote Patient Monitoring & Medical Imaging in the year 2010 and 2011. His research areas include planning and performance analysis of wireless networks and medical image analysis for automated diagnosis. He has more than 60 publications in international journals and proceedings. He has been awarded by various state and national agencies for his contribution to research and academics. He is also serving as reviewer for several reputed international journals.

Dr. Chandramani Kishore Singh is currently an assistant professor with the department of electronic systems engineering, Indian Institute of Science, Bengaluru. He received M.E. and Ph.D. degrees in electrical communication engineering from the Indian Institute of Science, Bengaluru, India, in 2005 and 2012, respectively. He worked as a wireless communications engineer in ESQUBE Communications Solutions Pvt. Ltd., Bengaluru, from 2005 to 2006. He was a post-doctoral researcher with TREC, a joint research team between INRIA Rocquencourt and ENS Paris from 2012 to 2013, and with the Coordinated Science Laboratory, University of Illinois at Urbana Champaign, USA, from 2013 to 2014. His research interests include communication networks, data centers, and smart grids. He has published more than 30 papers in respected international journals and conferences. Dr. Chandramani has also received the Microsoft Research India Rising Star Award in 2011.

Dr. Ayush Goyal is working as assistant professor in the department of electrical engineering and computer science at Texas A&M University, Kingsville, Texas. He completed his B.S. in electrical engineering from Boise State University (BSU),

Boise, USA and Ph.D. in computer Science from Oxford University, Oxford, UK. He was a postdoctoral research fellow in the department of computer science, Tulane University, New Orleans, USA. His areas of research interest are neurological disease prediction, brain MRI image analysis and bio-informatics for connected healthcare. He has more than 40 publications in international journals and proceedings. He was awarded Clarendon scholarship to pursue Ph.D. at Oxford University.

Benign–Malignant Mass Characterization Based on Multi-gradient Quinary Patterns

Rinku Rabidas, Romesh Laishram, and Amarjit Roy

Abstract This paper introduces a new descriptor, multi-gradient quinary pattern (M-GQP), for the categorization of breast masses as malignant or benign. The proposed attributes measure local information via local quinary pattern (LQP) based on a five-level encoding scheme from the gradient images obtained using Sobel operator having eight distinct masks at different directions. The gradient magnitude and angle image features provide better consistency and stability in high texture regions like edges and micro-information in different orientations, respectively. The assessment is performed using the mammographic images of the mini-MIAS dataset. A group of salient discriminators are opted via stepwise logistic regression technique, and a cross-validation method with tenfold is leveraged along with Fishers linear discriminant analysis as a classifier to avoid any bias. An Az value of 0.97 with an accuracy of 90.26% is achieved as the best outcome which is further compared with some of the competing methods in the literature.

Keywords Breast cancer · Mammogram · Mass · Classification · Multi- gradient pattern

R. Rabidas (✉)
Department of Electronics and Communication Engineering, Assam University, Silchar, India
e-mail: rabidas.rinku@gmail.com

R. Laishram
Department of Electronics and Communication Engineering, Manipur Institute of Technology, Takyelpat, India
e-mail: romeshlaishram@gmail.com

A. Roy
Department of Electronics and Communication Engineering, BML Munjal University, Gurgaon, India
e-mail: royamarjit90@gmail.com

R. Agrawal et al. (eds.), *Advances in Smart Communication and Imaging Systems*,
Lecture Notes in Electrical Engineering 721,
https://doi.org/10.1007/978-981-15-9938-5_1

1 Introduction

Though rare in male, breast cancer is the most common cancer cases among women worldwide and the second most common type of cancer overall. According to the latest report, new instances of breast cancer registered in the year 2018 were over 2 million [1]. Identification and diagnosis of breast cancer at the preliminary stage is the sole way to improve the survival rate. Although different imaging modalities are available at present, the most preferred method of screening breast cancer is X-ray mammography because other imaging methods like magnetic resonance imaging (MRI) and computed tomography (CT) have their own limitations of being expensive and high radiations, respectively. Several abnormalities which include bilateral asymmetry, architectural distortion, calcification, and mass are the usual symptoms of breast cancer at their early stages. Among these, the identification and characterization of masses are always a tough task because of the variations in size, shape, and margin. In addition to it, the fatigue caused to the radiologists due to the continuous examinations of mammograms, there may be a possibility of human error which can affect severely. Thus, computer-aided detection (CADe) and computer-aided diagnosis (CADx) systems are evolved to support the radiologists as an alternative evaluator.

In general, a mass is determined as malignant or benign based on the shape, margin, and texture information. A round/oval-shaped, smooth edge, and less fatty tissues are considered as benign case in contrast to the malignant ones having undefined margin, non-uniform shape, and high-fat tissues. This hypothesis is exploited by the researchers to introduce different shape-, margin-, and texture-based features for mass classification [2–5]. Though shape [4] and margin information [5] renders significant efficiency, it suffers from the limitation of precise segmentation of masses which is difficult to achieve in case of automatic systems. Therefore, mostly texture-based attributes [2, 6, 7] are preferred in the CADx systems. A comparative study of various attributes based on local textural information for mass categorization is presented in [8]. Haralick's texture measures generated from gray-level co-occurrence matrix (GLCM) of the rubber band straightening transform (RBST) images, proposed by Sahiner et al. [7], reported an area under the receiver operating characteristic (ROC) curve (A_z value) of 0.94 utilizing 160 mammographic images. The oriented patterns are investigated via radial local ternary pattern (RLTP), proposed by Muramatsu et al., and observed an A_z value of 0.90 [9]. Multi-resolution analysis of angular patterns is evaluated for the classification and observed an A_z value of 0.86 with 433 DDSM images [6]. Local binary pattern (LBP) with Zernike moments has also been successfully evaluated on mass classification of 160 mammograms having an efficiency of 0.96 [10]. Rabidas et al. analyzed the discontinuities by Ripplet-II transform and observed an A_z value of 0.91 [11]. Local descriptor-based curvelet transform are also inspected to diagnose the masses which delivered an efficiency of 0.95 with 200 mammograms [3]. Though various methods of mass characterization are reported in the literature, none assures complete success. Hence, in this paper, a new texture feature, multi-gradient quinary pattern (M-GQP), is proposed where

local measures are computed from the gradient images using LQP which offers more consistency in measuring gradient information from uniform and near-uniform areas. In addition, the extracted descriptors are also robust to illuminations. The gradient images, in both magnitude and angle, are obtained using Sobel operator having eight distinct masks at different directions as of result it provides better resolution in edge regions in addition to the micro-information at different orientations.

The paper is arranged as follows: The introduction of the mini-MIAS database is briefly provided in Sect. 2 followed by the methodology for mass classification in Sect. 3. The details about the experimental setup and the assessment of the result are discussed in Sect. 4. Lastly, the paper is concluded with the future scope of work in Sect. 5.

2 Database

To assess the proficiency of the introduced attributes, several experiments are performed utilizing the mammographic screenings of the mini-MIAS database—a widely used database by the researchers. This database is collected and managed by the Mammographic Image Analysis Society, London, UK [12]. The size of the mammograms is 1024×1024 and is digitized at 200 μm/pixel with 8 and 16 bits/pixel as gray-level resolution. Excluding the other anomalies, out of 59 mass cases, 20 malignant and 38 benign cases are selected in the present work. The annotations of the anomalies are attached along with the database.

3 Methodology

Since the texture of malignant and benign masses varies remarkably, in this paper, the discriminating textural information is measured via the proposed attributes, multi-gradient quinary patterns, for the determination of mammographic masses as malignant or benign. From the extracted descriptors, a subset of optimal features is opted out using a feature selection technique followed by a classifier for evaluation of the introduced attributes. The schematic layout of the proposed approach for benign–malignant mass categorization is demonstrated in Fig. 1.

3.1 Selection of ROIs

The distance between text and figure should be about 8 mm, and the distance between figure and caption about 6 mm. The annotations defining the mass lesions are provided along with the mini-MIAS database where the anomalies are marked by a circle with

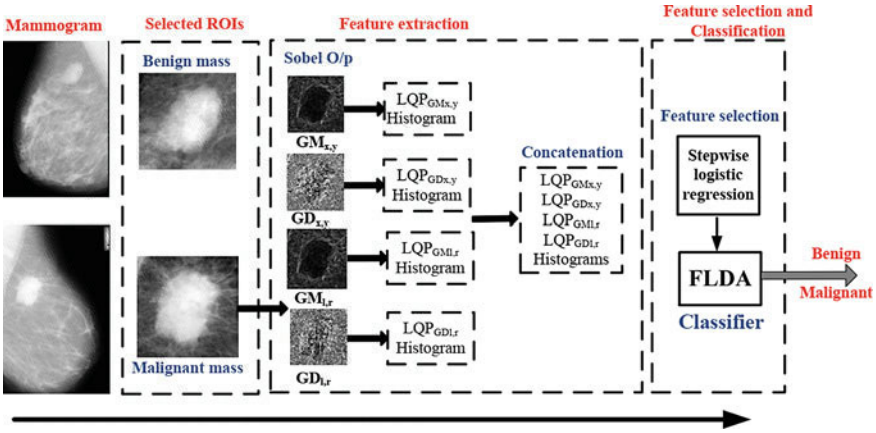

Fig. 1 Schematic layout of the introduced approach for benign–malignant mass classification

a predefined radius that encloses the mass lesion with its center at the middle. Considering 10 pixels more to the predefined radius, a region in square shape, covering the complete mass region, is chosen and termed as region of interests (ROIs). The sample images of the selected ROIs for both the malignant and benign masses are shown in selected ROIs section of Fig. 1.

3.2 Feature Extraction

Since features perform a key role in CADx systems, computation of salient attributes is also a challenging task. Considering the fact that the texture of malignant and benign masses varies remarkably, thus, in this study, a new descriptor, multi-gradient quinary pattern (M-GQP), is proposed where local information based on a five-level encoding scheme is measured from the gradient images. The gradient magnitude image measures render high consistency and stability in high texture regions like edges against the normal texture images in contrast to the gradient angle image which provides micro-information in different orientations. Moreover, the attributes extracted from gradient images are also robust to illuminations. Being simple, effective, and computationally efficient, Sobel operator is preferred with eight different masks at distinct directions (see Fig. 2) to obtain the two types of gradient images in *lr* and *xy* directions [13].

The convolution operation of an image patch with the east (e) and north (n) Sobel masks gives gradient relations of magnitude and angle along xy direction of the center pixel.

$$\begin{aligned} G_x(e) &= (p_o + 2p_1 + P_2) - (p_6 + 2p_7 + p_8) \\ G_y(n) &= (p_o + 2p_3 + P_6) - (p_2 + 2p_5 + p_8) \end{aligned} \tag{1}$$

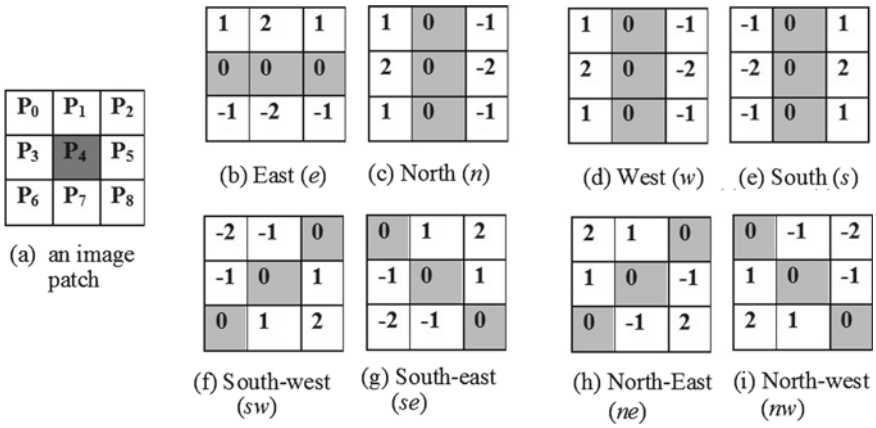

Fig. 2 Demonstration of different masks in different orientations

where $G_x(e)$ and $G_y(n)$ denote the gradient of the center pixel P_4 in horizontal and vertical directions, respectively. The gradient magnitude (GM_{xy}) and angle ($\theta_1(x, y)\, \varepsilon\, [0, \pi]$) components of the pixel P_4 along the north and east direction are calculated as follows:

$$GM_{xy}(e\_n) = |G_x(e)| + \left|G_y(n)\right|; \quad \theta_1(x, y) = GD_{xy}(e\_n) = \tan^{-1}\left(\frac{G_y(n)}{G_x(e)}\right) \tag{2}$$

The two other gradients using west (w) and south (s) Sobel masks can be obtained as:

$$G_x(w) = -G_x(e); \quad G_y(s) = -G_y(n) \tag{3}$$

Similarly, the gradient magnitude and angular components in the *lr* direction can be obtained through convolution of the image patch with southeast (se) and southwest (sw) Sobel masks as follows:

$$\begin{aligned} G_l(se) &= (p_1 + 2p_2 + P_5) - (p_3 + 2p_6 + p_7) \\ G_r(sw) &= (p_5 + 2p_8 + P_7) - (2p_0 + p_1 + p_3) \end{aligned} \tag{4}$$

where $G_l(se)$ and $G_r(sw)$ represent the gradient of the pixel P_4 along the left diagonal mask direction and right diagonal mask direction, respectively. In the similar way, by convolving with the northeast (ne) and northwest (nw) Sobel masks, we can calculate the other two gradients in the *lr* direction, but due to mirror symmetry it can be obtained as follows:

$$G_l(\mathrm{nw}) = -G_l(\mathrm{se}); \quad G_l(\mathrm{ne}) = -G_l(\mathrm{sw}) \tag{5}$$

Then, the gradient magnitude (GM_{lr}) and angle ($\theta_2(l, r)\, \varepsilon\, [0, \pi]$) of the pixel P_4 in the southwest and southeast direction are calculated as follows:

$$GM_{lr}(\text{se\_sw}) = |G_l(\text{se})| + |G_r(\text{sw})|; \quad \theta_2(l, r) = GD_{lr}(\text{se\_sw}) = \tan^{-1}\left(\frac{G_l(\text{se})}{G_r(\text{sw})}\right) \tag{6}$$

The different illustrations of malignant and benign masses in terms of gradient magnitude and angle representations are shown in Fig. 4.

These gradient images are further utilized to extract local measures via local quinary pattern (LQP) which offers consistency in near-uniform as well as uniform regions. Due to the five-level encoding scheme of LQP, it overcomes the limitations of LBP and its extended version local ternary pattern (LTP) [14]. The expression for five-level encoding of the texture image along with its splitting in different LBPs is given below:

$$d\left(I_p, I_c, T_1, T_2\right) = \begin{cases} +2, & I_p \geq (I_c + T_2) \\ +1, & (I_c + T_1) \leq I_P < (I_c + T_2) \\ 0, & (I_c - T_1) \leq I_P < (I_c + T_1) \\ -1, & (I_c - T_2) \leq I_P < (I_c - T_1) \\ -2, & \text{otherwise} \end{cases};$$

$$d_l(x) = \begin{cases} 1, & x = l, \quad l\varepsilon[-2, -1, 0, +1, +2] \\ 0 & \text{otherwise} \end{cases} \tag{7}$$

where I_c represents the intensity of the center pixel with I_p as its neighboring pixels. T_1 and T_2 are the thresholds for five-level quantization of the neighboring pixels which is further decomposed to observe LBPs as shown in Fig. 3. The histogram of LBPs obtained from the different gradient images (both angle and magnitude) at various orientations is concatenated to configure the final set of features of that image

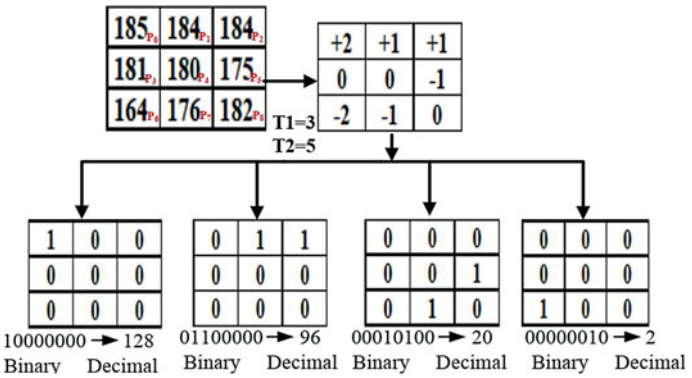

Fig. 3 Illustration of five-level code generation for LQP

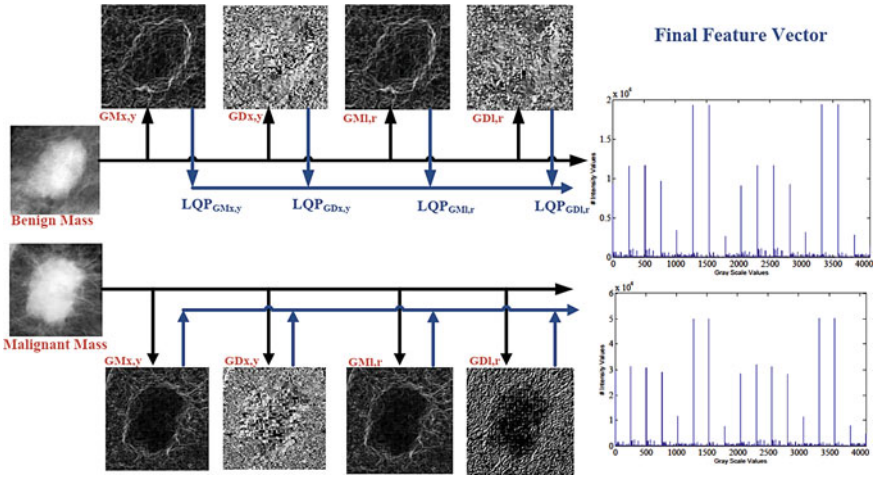

Fig. 4 Different illustrations of malignant and benign masses

(see Fig. 4) having length as 16×2^{P} where P defines the number of neighboring pixels. The distance between text and figure should be about 8 mm.

3.3 Selection of Features and Categorization

A large number of attributes are measured from the feature extraction step where all the computed measures do not carry remarkable discriminating potential for the determination of masses as malignant or benign. Moreover, it may lead to over-fitting problem. Hence, to filter the significant features, stepwise logistic regression technique [15] is employed. Being simple and effective, Fisher's linear discriminant analysis (FLDA) [16] is utilized as a classifier for decision making.

4 Experimental Setup, Results, and Discussion

The assessment of the introduced CADx system is carried out using MATLAB software on a personal computer. It comprises Intel(R) Core^{TM} i3 processor with 2.27 GHz frequency and 4 GB RAM. The performance evaluation matrix includes accuracy (A_{cc}) in percentage and A_z value to examine the efficiency of the proposed features. To avoid bias, if any, in the CADx system, cross-validation technique with tenfold is incorporated along with FLDA which is repeated for ten times and finally, the average of all the runs is reported as the outcome of the system.

Table 1 Average of accuracy (A_{cc}) and A_z value for proposed feature set having different values of thresholds—T_1 and T_2

Feature set (T_1, T_2)	A_z	A_{cc} (%)	*#FS**
M-GQP$_{1,3}$	**0.97 ± 0.02**	**90.26 ± 0.02**	5
M-GQP$_{1,4}$	0.90 ± 0.01	80.96 ± 0.01	6
M-GQP$_{1,5}$	0.93 ± 0.01	88.90 ± 0.01	5
M-GQP$_{2,4}$	0.96 ± 0.01	87.83 ± 0.02	5
M-GQP$_{2,5}$	0.81 ± 0.02	78.90 ± 0.03	6
M-GQP$_{3,5}$	0.91 ± 0.01	85.93 ± 0.02	6
M-GQP$_{3,6}$	0.89 ± 0.01	84.40 ± 0.02	7

*# *FS* indicates number of features selected
Bold indicates the best results in the table

The performance evaluation is conducted by varying the thresholds—T_1 and T_2 while keeping the parameters, R and P, constant with values 1 and 8, respectively, to avoid larger feature set. The final outcome of the proposed features with all the variations is provided in Table 1 where it can be noticed that unit difference in threshold values offers better efficiency and an A_z value of 0.97 with an accuracy of 90.26% is achieved as the best result. This optimum output is further compared with other competing methods reported in the literature as listed in Table 2 where it clearly establishes its supremacy over other techniques. Moreover, a comparison of the ROC curves with the proposed attributes against LBP [17], Haralick's [18], and histogram of oriented (HoG) [19] pattern features having an efficiency of 0.91, 0.68, and 0.93, respectively, is also illustrated in Fig. 5 which effectively demonstrates the superiority of the introduced descriptors.

Table 2 Proposed approach is compared with other recently developed competing schemes in terms of A_z value

Methods	A_z
M-GQP$_{1,3}$ (proposed)	**0.97**
Nascimento et al. [20]	0.96
Rabidas et al. [11]	0.91
Muramatsu et al. [9]	0.90
Serifovic-Trbalic et al. [21]	0.89
Midya and Chakraborty [6]	0.86

Bold indicates the best results in the table

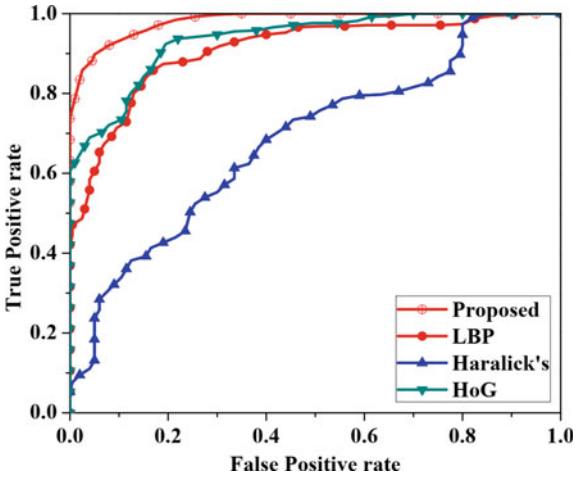

Fig. 5 Illustration of different ROC curves observed with various feature sets

5 Conclusion

In the present work, a new texture attribute, M-GQP, is introduced for the determination of breast masses as malignant or benign. Gradient images obtained after employing eight different masks of Sobel operator in various directions provide microscopic information along with better consistency in the high texture lesions like edges due to which it possesses significant categorizing potential in benign–malignant mass classification and outperforms some of the competing technique in the literature. The larger feature set is the limitation of this methodology which can be mitigated by using efficient feature selection technique. Hence, the authors are in a process to examine a suitable combination of feature selection technique and classifier on other larger databases.

References

1. Fund WCR (2019) Breast cancer statistics. https://www.wcrf.org/dietandcancer/cancertrends/breast-cancer-statistics. Accessed on Apr 2019
2. Rabidas R, Midya A, Chakraborty J (2018) Neighborhood structural similarity mapping for the classification of masses in mammograms. IEEE J Biomed Health Inform 22:826–834
3. Rabidas R, Midya A, Chakraborty J, Sadhu A, Arif W (2018) Multi-resolution analysis using integrated microscopic configuration with local patterns for benign malignant mass classification. In: Proceedings of SPIE medical imaging, p 105752N
4. Tahmasbi A, Saki F, Shokouhi SB (2011) Classification of benign and malignant masses based on Zernike moments. Comput Biol Med 41:726–735
5. Wei CH, Chen SY, Liu X (2012) Mammogram retrieval on similar mass lesions. Comput Methods Programs Biomed 106:234–248

6. Midya A, Chakraborty J (2015) Classification of benign and malignant masses in mammograms using multi-resolution analysis of oriented patterns. In: 12th international symposium on biomedical imaging (ISBI), Apr 2015, pp 411–414
7. Sahiner BS, Chan HP, Petrick N, Helvie MA, Goodsitt MM (1998) Computerized characterization of masses on mammograms: the rubber band straightening transform and texture analysis. Med Phys 24:516–526
8. Rabidas R, Midya A, Chakraborty J, Arif W (2016) A study of different texture features based on local operator for benign-malignant mass classification. Procedia Comput Sci 93:389–395 (2016) (Proceedings of the 6th International Conference on Advances in Computing and Communications)
9. Muramatsu C, Hara T, Endo T, Fujita H (2016) Breast mass classification on mammograms using radial local ternary patterns. Comput Biol Med 72:43–53
10. Laroussi M, Ben Ayed N, Masmoudi A, Masmoudi D (2013) Diagnosis of masses in mammographic images based on Zernike moments and Local binary attributes. In: World congress on computer and information technology (WCCIT), pp 1–6
11. Rabidas R, Chakraborty J, Midya A (2016) Analysis of 2D singularities for mammographic mass classification. IET Comput Vis 11(1):22–32
12. Suckling J (1994) The mammographic image analysis society digital mammogram database exerpta medica. Int Congr Ser 1069:375–378
13. Al-Sumaidaee S, Abdullah M, Al-Nima R, Dlay S, Chambers JA (2017) Multigradient features and elongated quinary pattern encoding for image-based facial expression recognition. Pattern Recogn 71:249–263
14. Nanni L, Lumini A, Brahnam S (2012) Survey on LBP based texture descriptors for image classification. Expert Syst Appl 39:3634–3641
15. Ramsey FL, Schafer DW (1997) The statistical sleuth: a course in methods of data analysis. Duxbury Press, CA
16. Duda RO, PH, Stork GD (2001) Pattern classification, 2nd edn. Wiley Interscience, New York
17. Ojala T, Pietikainen M, Maenpaa T (2002) Multiresolution gray-scale and rotation invariant texture classification with local binary patterns. IEEE Trans Pattern Anal Mach Intell 24:971–987
18. Haralick R, Shanmugam K, Dinstein I (1973) Textural features for image classification. IEEE Trans Syst Man Cybern 3:610–621
19. Pomponiu V, Hariharan H, Zheng B, Gur D (2014) Improving breast mass detection using histogram of oriented gradients. In: SPIE medical imaging—2014: computer aided diagnosis, vol 9035, Mar 2014, pp 90351R–90351R
20. do Nascimento MZ, Martins AS, Neves LA, Ramos RP, Flores EL, Carrijo GA (2013) Classification of masses in mammographic image using wavelet domain features and polynomial classifier. Expert Syst Appl 40:6213–6221
21. Serifovic-Trbalic A, Trbalic A, Demirovic D, Prljaca N, Cattin P (2014) Classification of benign and malignant masses in breast mammograms. In: 37th international convention on information and communication technology, electronics and microelectronics (MIPRO), May 2014, pp 228–233

Improved Switching Vector Median Filter for Removal of Impulse Noise from Color Images

Amarjit Roy, Snehal Chandra, and Rinku Rabidas

Abstract Image noise is defined as the random variation of color information or intensity in images. It is recognized as a type of electronic noise. Impulse noise is a "high level-low level" noise that affects an image abruptly. A filtering technique defined as an improved switching vector median filter (ISVMF) is proposed for removing impulse noise from color images in this manuscript. The performance analysis has been done for varied noise densities. Though performance has been shown in terms of Lena images, it delivers improved results irrespective of variation of images. The performance comparison has been done on the basis of standard metrics like peak signal to noise ratio (PSNR) and structural similarity index (SSIM), etc. It is observed that the proposed improved switching vector median filter (ISVMF) provides better results both visually and statistically as compared to the other conventional filtering techniques. This better performance may be due to the fact that the threshold has been localized rather than generalized in the filter resulting in better homogeneity across the various sections of the image.

Keywords Image noise · Impulse noise · Vector median filter · ISVMF · PSNR · SSIM

A. Roy (✉) · S. Chandra
Depatment of Electronics and Communication, BML Munjal University, Gurgaon, Haryana, India
e-mail: royamarjit90@gmail.com

S. Chandra
e-mail: snehalchandra31@gmail.com

R. Rabidas
Depatment of Electronics and Communication, Assam University, Silchar, Assam, India
e-mail: rabidas.rinku@gmail.com

R. Agrawal et al. (eds.), *Advances in Smart Communication and Imaging Systems*,
Lecture Notes in Electrical Engineering 721,
https://doi.org/10.1007/978-981-15-9938-5_2

1 Introduction

An image is a visual representation that has been stored and created in an electronic form. For image processing, different types of filtering techniques are used depending upon the requirements. The most traditional approach in this regard is considered as the application of median filter. This filter is a single-step filtering technique. It is applied on every pixel of a gray image irrespective of whether it is corrupt or not. The median of a given kernel is found out and the pixel under operation gets substituted by the calculated median. The principle of VMF filter is discussed in this section that is applicable for R-G-B images in which the pixel comprises of three components namely red (R), green (G), and blue (B). This filtering technique determines the vector distance between the corrupt pixels with each pixel in a given kernel and then replaces the corrupt pixel with the least vector distance. This is done in order to maintain the homogeneity of an image. The vector distance is calculated by the following general formula given as:

$$d = \sqrt{(XR^* - XR)^2 + (XB^* - XB)^2 + (XG^* - XG)^2} \tag{1}$$

where, the pixel to be operated is defined by: X^* and using the pixel X, the vector distance is being determined. The major drawback of the conventional VMF filtering technique that it operates on every pixel irrespective of whether it is corrupt or not which results in unnecessary wastage of time and machine cycles.

A lot of image denoising algorithms are available in the literature for removing impulses from corrupted images. An adaptive switching median (ASWM) filter [1] works on a localized threshold value which delivers improved results considering parameters like MAE and PSNR in comparison with median filtering algorithms. A SVM-based fuzzy filter [2] showed a great improvement in PSNR for the images corrupted by high density noise. An advanced technique for removing impulse noise with adaptive dual thresholds [3] has been further improved by the introduction of an adaptive support vector-based classification filter (ASVC) [4]. It is suggested to revise the existing techniques by implementation of new methodology in them [5]. A mathematical tool derived using robust estimation theory is used to develop nonlinear filters to provide excellent robustness properties [6]. In center weighted median (CWM), more weight is being provided at the central pixel so as to achieve superior performance. It is observed that more image information is restored with better visual perception [7]. A filter having switching procedure based on the local measurements of impulses yielded better results [8]. In another technique, using Laplacian operator, minimum value from the obtained convolutions is calculated in one-dimensional way [9]. Noise ranking switching filter (NRSF) outperforms several advanced filtering techniques that preserves more textural information with more edge details [10]. The switching bilateral filter (SBF) incorporates an improved noise detector that is utilized to detect both impulse as well as Gaussian noise [11]. In boundary discriminative noise detection (BDND), two different noise detection

techniques have been incorporated which in turn improves the performance not only in detection but also in noise removing capability [12]. A superior technique for removal of impulses from gray images is based on SVM classification has been proposed by Roy et al. [13]. Region adaptive fuzzy filter that utilizes the channel difference information for re-construction of channel information has been proposed in the paper [14]. This filtering technique is very useful for random valued impulse noise.

This research paper proposes a dynamic and robust image filtering technique for getting the image of optimum quality. The section organization is as follows; Sect. 2 comprises of the proposed filtering technique implementation, Sect. 3 elaborates results and discussions, and Sect. 4 concludes the chapter.

2 Improved Switching Median Filter (ISVMF)

The proposed methodology has incorporated the switching scheme of adaptive switching median (ASWM) filter [1] with vector median filter. First, detection is done according to ASWM and after that a VMF is processed on each pixels so as to remove the noise. At low density impulse noise, VMF with (5×5) is applicable. In contrast, at high density impulse noise, VMF with (7×7) window offers enhanced performance irrespective of images.

Detection of noise [1] is started with the calculation of the weighted standard deviation and weighted mean in the current kernel. The weights are in an inverse relation with the distance between weighted mean of pixels in the given kernel and pixel under operation. In each kernel, in an iterative manner the weighted mean is calculated. Then, by calculating the weighted standard deviation, the localized threshold is determined. This algorithm is explained in the following steps:-

Initial Stage: Consider a window W of size $[(2Q+1) \times (2Q+1)]$ whose weighted mean.

M_w is calculated for the pixels around the pixel under operation.

$$M_{w(i,j)} = \frac{\sum_{k,l} W_{k,l}\, X_{i+k,j+l}}{\sum_{k,l} W_{k,l}} \tag{2}$$

where $X_{i,j}$ is the pixel value and $W_{k,l}$ the weights. All these weights are equal to 1 at initial stage. The variation of index k and l is in the range of $[-Q, Q]$.

Step 1: The required weights are calculated as

$$W_{k,l} = \frac{1}{\left| X_{i+k,j+l} - M_w(i,j) + \delta \right|} \tag{3}$$

□ is a pre-determined small value, which is used by the denominator to avoid a possible indeterminate form. Then, a new weighted mean is determined by using (1).

Step 2: If, $|M_w(i,j)^t - M_w(i,j)^{t-1}| < \varepsilon$ where ε is an experimentally determined value, then the iteration is stopped, otherwise, start again from the first step.

($M_w(i,j)^t$ is the calculated weighted mean at any given iterative stage).

Next, the weighted standard deviation $\sigma_w(i,j)$ is given as:

$$\sigma_{w(i,j)} = \sqrt{\frac{\sum_{k,l} W_{k,l}\,(X_{i+k,j+l} - M_w(i,j))^2}{\sum_{k,l} W_{k,l}}} \tag{4}$$

The above steps are performed separately for each of the three components (red, blue, and green) of a pixel in a color image. Finally, ISVMF can be summarized in the following way:

1. Determine $\sigma_w(i,j)$ and $M_w(i,j)$, which are the weighted standard deviation and weighted mean respectively of the kernel comprising of the pixel under operation for each component of red, green, and blue.
2. The following rule is used for each of the RGB component of each pixel:

$$Y_{i,j} = \begin{cases} m_{i,j}, \text{ if} \left| X_{i,j} - M_{i,j} \right| > \alpha \times \sigma_w(i,j) \\ X_{i,j}, \text{ otherwise} \end{cases} \tag{5}$$

where $m_{i,j}$ is median of the kernel, α a given parameter and $\alpha \times \sigma_w(i,j)$ represents the localized threshold value. ISVMF is applied in a repetitive fashion. During each iteration stage in a given window, the threshold gets decreased. This is achieved by varying α value. Simulations performed on various standard images showed that the following strategy gives optimum results, which is given as:

$$\alpha_0 = 20; \alpha_{n+1} = \alpha_n \times 0.8 (n \geq 0) \tag{6}$$

where α_0 is the α parameter at initial stage and α_n the parameter in the nth step.

After detection of noise (Eqs. 2–6), VMF is processed over the image. An experiment has been performed for the selection of window size. Up to 40% of impulse noise VMF with 5×5 window is applicable, whereas beyond this a 7×7 window is applied. After completion of this stage, VMF is again applied so as to achieve final filtered image. This is done because some noisy pixels have not been detected in the earlier stage (Fig. 1).

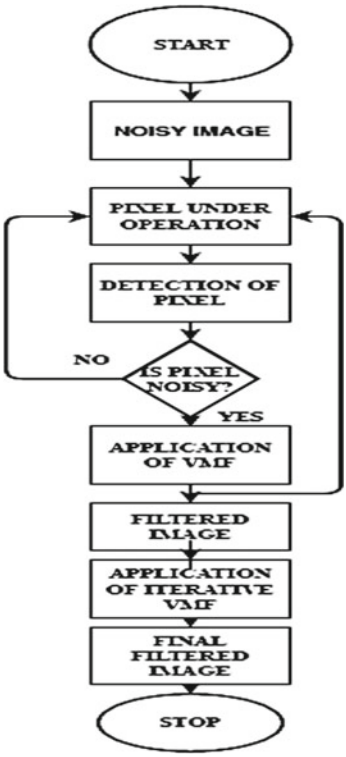

Fig. 1 Flowchart for the proposed filtering technique (ISVMF)

3 Results and Discussion

Under this section, we are doing a comparison of the performance of conventional VMF and ISVMF on the basis of the following standard parameters:

1. Mean square error (MSE)
2. Structural similarity index (SSIM)
3. Peak signal to noise ratio (PSNR).

Among these parameters, PSNR should be high, MSE should be low, whereas the values of SSIM should be more and nearer to 1 (Figs. 2, 3 and Tables 1, 2, 3, 4, 5).

After analyzing the mathematical and visual results, it was observed that a bigger window size performed because of the presence of more number of non-corrupt pixels due to which the noise density becomes less, resulting in a clearer image. It has been observed that Fig. 4b provides more improved performance in comparison with Fig. 4a with less blurring effect also. This was proved as the various standard parameters of image processing like PSNR, MSE, and SSIM were found to be better in those cases. Hence, the proposed ISVMF was found to be more efficient than the conventional VMF technique for filtering of impulse noise from color images.

Fig. 2 **a** Original "Lena" image, **b** original "Lena" image

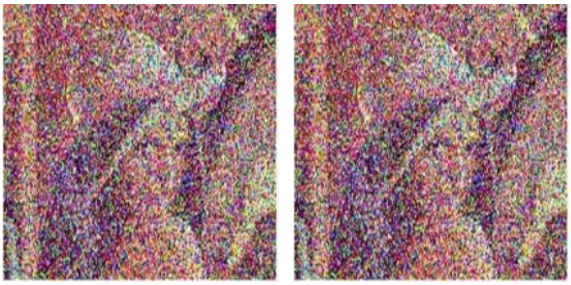

Fig. 3 **a** Image with 50% noise, **b** image with 50% noise

Table 1 Observation table for kernel size 5 * 5 of PSNR

Noise density	PSNR	
	VMF	ISVMF
20	17.6212	36.6632
30	16.6092	34.1920
40	13.5764	31.3951
50	11.6432	26.2427
60	9.7941	24.1143
70	8.2878	20.1392
80	7.1054	18.7065

4 Conclusion

After going through the different tables, observations, and the related parameters, we can conclude that if the noise density is low then a smaller window would provide us with an optimum quality image and if noise density is high, then in that case a larger window would provide with an optimum quality image. A better filter can be developed if a localized threshold is used rather than a generalized threshold in a